Convection in binary fluid mixtures with modulated heating

B. L. Smorodin[1,*] and M. Lücke[2]
[1]*Perm State University, 614990, Perm, Russia*
[2]*Institut für Theoretische Physik, Universität des Saarlandes, Postfach 151150, D-66041 Saarbrücken, Germany*
(Received 18 November 2008; published 25 February 2009)

The response behavior of strongly nonlinear binary fluid convection to temporal modulation of the heating is investigated for the case of a negative Soret coupling between temperature and concentration gradients. Finite difference numerical simulations are performed for ethanol-water parameters subject to realistic boundary conditions. Traveling waves with modulated amplitudes and phase velocities, subharmonic standing waves, and synchronously modulated patterns with fixed spatial phase are found as stable solutions. The hysteretic transitions between subcritical traveling and standing waves that coexist bistably with the quiescent fluid state are investigated. Various diagnostic analysis tools are used to elucidate the complex spatiotemporal and bifurcation properties that are ultimately caused by nonlinear advection and mixing of concentration being very strong.

DOI: 10.1103/PhysRevE.79.026315 PACS number(s): 47.20.Ky, 47.20.Lz, 47.54.−r

I. INTRODUCTION

Nonlinear dissipative systems that are driven sufficiently far away from thermal equilibrium show often self-organization [1]. Convection in binary miscible fluids like, e.g., ethanol-water is an example of such systems. It shows rich and interesting pattern formation behavior and it displays a wide range of phenomena related to instabilities, bifurcations, and self-organization with complex spatiotemporal behavior.

Compared to convection in one-component fluids like, e.g., pure water the spatiotemporal properties are far more complex. The reason is that concentration variations which are generated via thermodiffusion—the Soret effect—by externally imposed and by internal temperature gradients influence the buoyancy, i.e., the driving force for convective flow. The latter in turn mixes by advectively redistributing concentration. This nonlinear advection gets in developed convective flow typically much larger than the smoothening by linear diffusion—Péclet numbers measuring the strength of advective concentration transport relative to diffusion are easily O (1000). Thus, the concentration balance is strongly nonlinear giving rise to strong variations of the concentration field and to boundary layer behavior. In contrast to that, momentum and heat balances remain weakly nonlinear close to onset as in pure fluids implying only smooth and basically harmonic variations of velocity and temperature fields as of the critical modes.

Without the thermodiffusive Soret coupling between temperature and concentration any initial concentration deviation from the mean diffuses away and influences no longer the balances of the other fields. Hence, the feedback interplay between (i) the Soret generated concentration variations, (ii) the resulting modified buoyancy, and (iii) the strongly nonlinear advective transport and mixing causes binary mixture convection to be rather complex with respect to its spatiotemporal properties and its bifurcation behavior.

Here we consider the case of negative Soret coupling, $\psi < 0$, between temperature and concentration fields [2,3] when the lighter component migrates to the colder regions thereby stabilizing the density stratification in the quiescent, laterally homogeneous conductive fluid state. Then the above described feedback interplay generates oscillations. In fact the buoyancy difference in regions with different concentrations was identified already in [4] as the cause for traveling wave (TW) convection.

Oscillatory convection appears in a rather large variety: As transient growth of convection at supercritical heating, in spatially extended nonlinear TW and standing wave (SW) solutions that branch out of the conductive state via a common Hopf bifurcation, in spatially localized TW states, and in various types of fronts [1,5–23].

In this work we investigate spatially extended convection patterns consisting of straight rolls as they appear in narrow rectangular and annular channels. These structures can efficiently be described in the two-dimensional vertical x-z cross section in the middle of the channel perpendicular to the roll axes ignoring variations in axis direction. Furthermore, these convection structures have relevant phase gradients only in x direction thus causing effectively one-dimensional patterns [24]. For such structures we explore the effect of modulating the heating rate, i.e., the forcing mechanism that causes convection in the first place.

The influence of time-dependent gravitational accelerations or vibrations on the onset of Rayleigh-Benard convection was studied in [25,26]. The linear stability problem for the single component system was reduced to the damped Mathieu equation. It was shown that high-frequency vibrations can increase the stability of the quiescent state. Finite frequency vibrations, on the other hand, can destabilize the quiescent state by a resonance phenomena. The effect of modulating the temperatue of the horizontal boundaries on the threshold for onset of convection in a horizontal layer of a homogenous fluid was studied in Refs. [27–29]. In the quiescent basic state the temperature modulation drives heat waves that propagate diffusively between the boundaries of the layer.

*bsmorodin@yandex.ru

The convective instability of a pure fluid under vibrations or under a modulated temperature gradient can be related to two types of critical disturbances that are in general the first that get undamped: For a synchronous response the oscillation period of the convective disturbances coincides with the period of the external modulation. In the case of a subharmonic response the period of the latter is 2 times as large as the modulation period. The influence of temporal modulation on pattern formation and nonlinear dynamics in pure liquids was investigated experimentally [30], and theoretically [31]. A Lorenz-like model of the hydrodynamic equations was used in these investigations.

In comparison to pure fluid convection a richer and more interesting situation arises in binary mixtures when already in the absence of modulation oscillatory convection appears. Then two (symmetry degenerated) oscillating convective modes get undamped via a Hopf bifurcation and a SW solution and two left or right propagating TW solutions branch out of the quiescent basic state.

The purpose of the present paper is to present results of numerical simulations of strongly nonlinear convection in binary mixtures with negative Soret coefficient in the presence of finite-frequency temperature modulations with amplitudes of about 20% around the mean. We consider here the hysteretic case where the bifurcation of SW and TWs without modulation is backwards. We elucidate the spatiotemporal behavior and the bifurcation properties of different relaxed convective structures under temporal modulation and also transients between different solutions.

The paper is organized as follows: In Sec. II we describe the problem and the governing equations. In Sec. III we give a brief summary of the solutions in the unmodulated case before presenting in Sec. IV our results in the presence of modulation. The last section contains concluding remarks.

II. SYSTEM

Let us consider a horizontal plane layer of a binary fluid mixture that is oriented perpendicular to the vertical gravitational acceleration g. The fluid might be a mixture of water with the lighter component ethanol at a mean mass concentration $\bar{C}$. The layer is bounded by rigid, impervious and perfectly heat conducting parallel planes located at $z=0$ and $z=h$. Thus, h is the thickness of the layer. The upper boundary is kept at some fixed temperature T_u. The temperature T_l that is imposed at the lower boundary is modulated sinusoidally with frequency Ω according to

$$T_l(t) = T_u + \Delta T(1 + \delta \sin \Omega t). \tag{2.1}$$

The mean temperature difference is ΔT and its relative modulation amplitude is δ. We take T_u as the reference temperature $\bar{T}$ and we consider the (small) variations of the fluid density ρ due to temperature and concentration variations to be governed by the linear thermal and solutal expansion coefficients $\alpha=-\frac{1}{\rho}\frac{\partial \rho}{\partial T}$ and $\beta=-\frac{1}{\rho}\frac{\partial \rho}{\partial C}$, respectively. Both are positive for ethanol-water.

A. Equations

To describe convection in this system we use the balance equations for mass, momentum, heat, and concentration in Oberbeck-Boussinesq approximation which read in nondimensional form [21,33,34]

$$\boldsymbol{\nabla} \cdot \mathbf{v} = 0, \tag{2.2a}$$

$$\frac{\partial \mathbf{v}}{\partial t} + (\mathbf{v} \cdot \boldsymbol{\nabla})\mathbf{v} = -\boldsymbol{\nabla} p + \sigma \nabla^2 \mathbf{v} + \sigma R(T + C)\mathbf{e}_z, \tag{2.2b}$$

$$\frac{\partial T}{\partial t} + (\mathbf{v} \cdot \boldsymbol{\nabla})T = \nabla^2 T, \tag{2.2c}$$

$$\frac{\partial C}{\partial t} + (\mathbf{v} \cdot \boldsymbol{\nabla})C = L\nabla^2(C - \psi T). \tag{2.2d}$$

Here, $\mathbf{v}$ is the velocity field, $\mathbf{e}_z$ is the unit vector directed upward, and p is the pressure. T and C are scaled (cf. below) deviations of temperature and concentration from $\bar{T}$ and $\bar{C}$, respectively. Rayleigh number R, Prandtl number σ, Lewis number L, and separation ratio ψ are given by

$$R = \frac{g\alpha \Delta T h^3}{\nu \kappa}, \quad \sigma = \frac{\nu}{\kappa}, \quad L = \frac{D}{\kappa},$$

$$\psi = -\frac{\beta \kappa_T}{\alpha \bar{T}} = S_T \bar{C}(1 - \bar{C})\frac{\beta}{\alpha}. \tag{2.3}$$

Here ν is the kinematic viscosity, κ is the thermal diffusivity, and D is the concentration diffusion constant of the mixture while $k_T=\bar{T}\bar{C}(1-\bar{C})S_T$ is the thermodiffusion coefficient [33] and S_T is the Soret coefficient. Furthermore, the following scales have been used in Eqs. (2.2): Length, h; time, h^2/κ; velocity, κ/h; temperature, ΔT; concentration $\alpha \Delta T/\beta$; pressure, $\rho\kappa^2/h^2$.

We solved the field equations (2.2) for two-dimensional (2D) roll convection with axes oriented in y direction. To that end we introduced the stream function Ψ and the vorticity φ which are connected to the velocity field in the following way:

$$\mathbf{v} = \left(\frac{\partial \Psi}{\partial z}, 0, -\frac{\partial \Psi}{\partial x}\right), \quad \varphi = (\boldsymbol{\nabla} \times \mathbf{v})_y. \tag{2.4}$$

Then the partial differential equations (2.2) are transformed into

$$\varphi = -\nabla^2 \Psi, \tag{2.5a}$$

$$\frac{\partial \varphi}{\partial t} + \frac{\partial \Psi}{\partial z}\frac{\partial \varphi}{\partial x} - \frac{\partial \Psi}{\partial x}\frac{\partial \varphi}{\partial z} = \sigma \nabla^2 \varphi + \sigma R \frac{\partial (T + C)}{\partial x}, \tag{2.5b}$$

$$\frac{\partial T}{\partial t} + \frac{\partial \Psi}{\partial z}\frac{\partial T}{\partial x} - \frac{\partial \Psi}{\partial x}\frac{\partial T}{\partial z} = \nabla^2 T, \tag{2.5c}$$

$$\frac{\partial C}{\partial t} + \frac{\partial \Psi}{\partial z}\frac{\partial C}{\partial x} - \frac{\partial \Psi}{\partial x}\frac{\partial C}{\partial z} = L\nabla^2(C - \psi T). \tag{2.5d}$$

1. Boundary conditions

The horizontal boundaries at $z=0,1$ are taken to be no-slip ($\mathbf{v}=0$) and impervious so that

$$\Psi = 0, \quad \frac{\partial \Psi}{\partial z} = 0, \quad \frac{\partial C}{\partial z} - \psi \frac{\partial T}{\partial z} = 0. \tag{2.6}$$

The temperatures at the boundaries are $T(0)=1+\delta \sin \Omega t$ and $T(1)=0$, respectively.

Laterally we impose periodic boundary conditions, $f(x,z,t)=f(x+\lambda,z,t)$, on all fields $f=\Psi,\varphi,T,C$ with $\lambda=2$ throughout the paper. Thus, the wave number of the convection pattern $k=\pi$ is close to the critical one and close to the one that one typically observes for oscillatory convection rolls at negative ψ, say, in narrow annular containers.

2. Solution method

For solving the system of equations (2.5) an alternating-direction implicit scheme is used with central differences for the spatial derivatives and one-sided right differences for the time derivatives. This is a finite difference method of second order. The stream function was determined with an iterative method of successive over relaxation at each time step. Typically, a state of relaxed finite amplitude convective oscillations obtained at a particular set of parameters was used as initial condition for a run at another set of parameters.

3. Parameters

In this paper we consider mixtures with $L=0.01$, $\sigma=10$, and $\psi=-0.25$. This set of parameters is characteristic for and easily experimentally realizable with ethanol-water mixtures. The wave number of the convection rolls is $k=\pi$. The relative amplitude of the temperature modulation (2.1) of the lower boundary is $\delta=0.2$.

B. Diagnostic tools

To measure the intensity of the heating we use the reduced Rayleigh number $r=R/R_c^0$, where R_c^0 is the critical Rayleigh number for onset of pure-fluid convection with the critical wave number k_c^0. Linear stability theory predicts $R_c^0=1707.8$ and $k_c^0=3.116$. However, to compare our finite differences numerical results presented in this paper with experimental, analytical, or numerical ones we scale R by the threshold $R_c^0=1701.5$ of our numerical code. Most of the calculations are executed using grids of 47×31 nodes. A further mesh refinement to 82×61 nodes does not provide a significant improvement in the evaluation of oscillation characteristics and shows no relevant differences.

To monitor the convection intensity we use the Nusselt number

$$\mathrm{Nu}(t) = \int_0^\lambda \frac{\partial T(x,z,t)}{\partial z} dx, \tag{2.7}$$

say, at $z=1$ measuring the total vertical heat flux there. Furthermore, we monitor the maximum of the vertical flow field in the x-z cross section perpendicular to the roll axes

$$w_{\max}(t) = \max_{x,z} w(x,z,t) \tag{2.8}$$

as well as the time evolution of w at a fixed position x_0,z_0.

We also consider running time averages of various quantites $f(t)$ over some time interval, in particular over a period of the modulation $\tau=2\pi/\Omega$,

$$\langle f \rangle(t) = \frac{1}{\tau} \int_{t-\tau/2}^{t+\tau/2} f(t')dt', \tag{2.9}$$

as well as long-time averages

$$\langle f \rangle = \frac{1}{\mathcal{T}} \int_0^{\mathcal{T}} f(t)dt \tag{2.10}$$

with very large $\mathcal{T}$. The latter is used among others to determine the mean lateral velocity $\langle v_{ph} \rangle$ of the phase of w as measured by the time derivative of node locations of $w(x,z=1/2,t)$ at midheight of the fluid layer, $v_{ph}=dx_{(w=0)}/dt$. Thus,

$$\langle v_{ph} \rangle = [x_{(w=0)}(\mathcal{T}) - x_{(w=0)}(0)]/\mathcal{T}. \tag{2.11}$$

To elucidate the spatiotemporal complexity of the convective behavior and of the transitions between various regimes we have also studied lateral Fourier decompositions,

$$f(x,t) = f_0(t) + \mathrm{Re}\left(\sum_{n=1}^{\infty} \hat{f}_n(t) e^{-inkx} \right) \tag{2.12}$$

of the fields at midheight position, $z=1/2$. The behavior there is largely representative for all other z.

Finally we analyzed the evolution of the spatial variance of the concentration field in the layer. To that end we monitored the mixing number

$$M = \sqrt{\overline{C^2}/\overline{(C_{\mathrm{cond}}^0)^2}}, \tag{2.13}$$

of the concentration field. Here, the overbar implies a spatial average over the layer. The Soret induced conductive concentration profile $C_{\mathrm{cond}}^0(z)=-\psi(z-1/2)$ in the quiescent ($\mathbf{v}=0$) unmodulated ($\delta=0$) layer varies from $-\psi/2$ at the top boundary to $\psi/2$ at the bottom one with $\overline{(C_{\mathrm{cond}}^0)^2}=\psi^2/12$. Note that M lies in the interval $0<M<1$. The better the fluid is mixed advectively the smaller is the mean-square deviation $\overline{C^2}$ of the concentration. In the unmodulated conductive state without advective mixing $M=1$ while $M=0$ in a perfectly homogenized mixture with $C=0$.

III. STATIONARY HEATING

Here we briefly recall some of the bifurcation and spatiotemporal properties of the laterally extended convective states in mixtures for our parameters of Sec. II A 3 in the absence of modulation, $\delta=0$. See Refs. [5,20] for details.

The convective instability of the ethanol-water mixture arises as a Hopf bifurcation at the reduced Rayleigh number $r_{\mathrm{osc}}=1.335$ with a Hopf frequency $\omega_H(k=\pi,r_{\mathrm{osc}})=11.246$. Our finite-differences numerical method, on the other hand, yields $r_{\mathrm{osc}}=1.318$. Thin lines in Fig. 1(a) show for $\delta=0$ the bifurcation diagrams of maximal vertical flow velocity $w_{\max}$

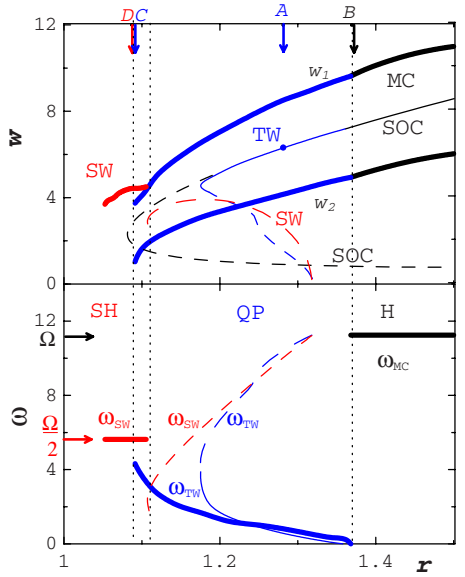

FIG. 1. (Color online) Bifurcation diagrams of laterally extended convective states with wave number $k=\pi$ in binary fluid mixtures as functions of reduced Rayleigh number r. Thick lines refer to temperature modulation (2.1) of the lower boundary with relative amplitude $\delta=0.2$ and frequency $\Omega=\omega_H=11.246$. Vertical dotted lines mark boundaries of subharmonic (SH), quasiperiodic (QP), and harmonic (H) response to modulation in the form of SWs, TWs, and phase fixed modulated convection (MC), respectively. Under modulation the maximal vertical velocity $w_{\max}(t)$ defined in Eq. (2.8) oscillates between the thick lines labeled by w_1 and w_2, respectively, in (a). Thick lines in (b) denote the largest Fourier contribution in the frequency spectrum of $w(t)$. Arrows labeled A, B, C, D locate states that are discussed in more detail in the text. Thin lines refer to the maximal vertical flow velocity (a) and the frequency (b) of the reference states under stationary heating, $\delta=0$, with full (dashed) ones denoting stable (unstable) solutions. The dot in (a) is explained in the text. Parameters are $L=0.01$, $\sigma=10$, $\psi=-0.25$.

versus reduced Rayleigh number r for the traveling wave (TW) solution, the stationary overturning convection (SOC) solution, and the standing wave (SW) solution. The SOC solution branch is disconnected from the quiescent conductive state. Both, the TW and SW solutions bifurcate backwards out of the conductive state at $r_{\rm osc}$.

When following the solution branches SWs remain unstable while TWs gain stability in a saddle-node bifurcation at $r_S^{\rm TW}=1.175$. So, for $r<r_S^{\rm TW}$ convection in the unmodulated fluid layer dies out whereas above $r_S^{\rm TW}$ stable, strongly nonlinear TW convection exists. However, this stable TW solution branch ends at $r^*=1.36$ by merging with zero frequency in the SOC branch thereby transferring its stability to the SOC solution.

The thin lines in Fig. 1(b) show the bifurcation behavior of the frequency ω of the nonlinear TW and SW solutions for stationary heating, $\delta=0$. These frequencies are largest at the Hopf bifurcation treshold $r_{\rm osc}$. There one has $\omega_H=11.246$. Then, upon moving with increasing flow amplitude $w_{\max}$ along the solution branches in Fig. 1(a) the frequency decreases. Thus, e.g., the TW frequency at the saddle, $r_S^{\rm TW}=1.175$, has dropped already to $\omega_S^{\rm TW}=3.88$. Continuing further—now with increasing r—along the upper TW solution branch of Fig. 1(a) the TW frequency decreases further until it reaches zero at $r^*=1.36$ where the TW branch ends in a drift instability of the SOC branch.

It should be noted that the size of the Soret induced concentration gradients determine the magnitude of the restoring force for oscillatory convection, i.e., the frequencies of TWs and SWs (Fig. 3 of Ref. [20] shows that the relation $\omega/\omega_H \sim M$ holds for TWs as well as for SWs): Above r^* the heating has become so large that the advective mixing is strong enough to reduce the Soret induced concentration gradients to effectively zero so that $\omega=0$ in the SOC state. On the other hand, when moving downwards along the TW solution branch in Fig. 1(a) all the way to $r_{\rm osc}$ the flow intensity and with it the advective mixing decreases all the way to zero, the Soret induced concentration gradients and with it the mixing number M increase to their maximum value $M=1$ in the quiescent conductive state, and the restoring force for oscillations, i.e., the oscillation frequency increases to its maximal value ω_H at $r_{\rm osc}$.

IV. MODULATED HEATING

Modulation of the thermal driving force for convection with the relative amplitude of $\delta=0.2$ considered here generates a very rich response behavior. This is not really surprising since already the unmodulated convective states are strongly nonlinear with quite complex spatiotemporal behavior of the concentration field that is largely determined by strong advective transport. Furthermore, for most of the r values shown in Fig. 1 the reduced Rayleigh number

$$r(t) = r[1 + \delta \sin(\Omega t)] \tag{4.1}$$

covers an interval from well below the lower existence limit of unmodulated nonlinear TWs at $r_S^{\rm TW}=1.175$ to well above its upper existence limit at $r^*=1.36$. Thus, an important criterion to classify the response behavior is, e.g., how long the actual driving $r(t)$ (4.1) remains during the modulation cycle below $r_S^{\rm TW}$ where unmodulated convection would decay into the conductive state or below the saddle location $r_S^{\rm SW}=1.11$ of the unmodulated unstable SWs.

In this paper we consider "large frequency" modulation in the sense that $r(t)$ does not stay too long subcritical, i.e., below $r_S^{\rm TW}$ so that the advection amplitudes remain of sufficient size during the whole modulation cycle. In a second paper we address the behavior at lower frequencies. Here, we investigate the range $0.4\omega_H \leqslant \Omega \leqslant \omega_H$ in which we found the qualitative similar characteristics of a "large frequency" response and we discuss in detail the case $\Omega=\omega_H=11.246$ as a representative example for this behavior.

Depending on the size of r this convective response is subharmonic in the form of a stable SW, quasiperiodic in the form of a modulated TW, or harmonic in the form of phase fixed modulated convection. All these states explored here display in the driving range of Fig. 1 the mirror-glide symmetry

$$f(x,z;t) = -f(x+\lambda/2, 1-z; t) \tag{4.2}$$

with f denoting Ψ, φ, T, or C that is also observed in TWs, SWs, and SOCs under stationary heating [5,20].

The quasiperiodic modulated TWs at larger driving have practically constant phase velocities with only their amplitudes being modulated. But with decreasing r the phase modulation and the modulation of the phase velocity increases.

Before we discuss all these properties in more detail in the Secs. IV B–IV F we shortly want to address the question of the relevant time scales.

A. Time scales

Consider first the time scales (measured in units of the vertical thermal diffusion time h^2/κ) for diffusive transport of momentum, heat, and concentration $(1/\sigma, 1, 1/L) = (0.1, 1, 100)$ and for vertical advection of these fields $1/w_{\max}$. So, for flow intensities $w_{\max} > 1$ that are typical for nonlinear convective states concentration is advection dominated and is not smoothened diffusively while the converse is true for the velocity field: The balance equation for momentum is weakly nonlinear (as long as the rate for advective momentum transport is small compared to the diffusive transport rate) while the balance equation for concentration is strongly nonlinear with its Peclet number, $w_{\max}/L$, being typically very large.

The external modulation period $\tau = 2\pi/\Omega \simeq 0.56$ is larger than the momentum diffusion time so that the velocity field has enough time to be smoothed out diffusively while the concentration field remains to be advection dominated. Note also that for most of the states investigated here $\tau > 1/w_{\max}$ so that even for such "large frequency" modulation the characteristic time for nonlinear advective transport is smaller than the modulation period. But Ω is larger by, say, a factor of 3 than the unmodulated TW and SW frequencies, ω_S^{TW} and ω_S^{SW}, respectively, near their respective saddle locations. So, in this respect we have a "large frequency" modulation.

Furthermore, τ is small compared to the decay time of a TW or SW initial state that is prepared with saddle characteristics (slightly) below r_S^{TW} or r_S^{SW}. Such decay dynamics will take place when the driving $r(t)$ stays long enough below the saddle locations. Thus, the smallness of τ relative to the decay time for this "large frequency" driving guarantees that $w_{\max}$ remains of significant size. In contrast to that, the flow amplitude can decay to very small values for "low frequency" driving since then $r(t)$ will be a long time below the saddle positions.

B. Amplitude modulated traveling waves

"Large frequency" temperature modulation enlarges the existence range of unmodulated TWs from $1.175 < r < 1.361$ to $1.091 < r < 1.368$ as indicated by the thick lines in Fig. 1. At the upper end of this r interval the phase velocity v_{ph} of the TWs is practically constant and only the amplitude is modulated. Then, with decreasing r also v_{ph} gets modulated as described in Sec. IV D. Here, we discuss first the case where the TWs are only amplitude modulated.

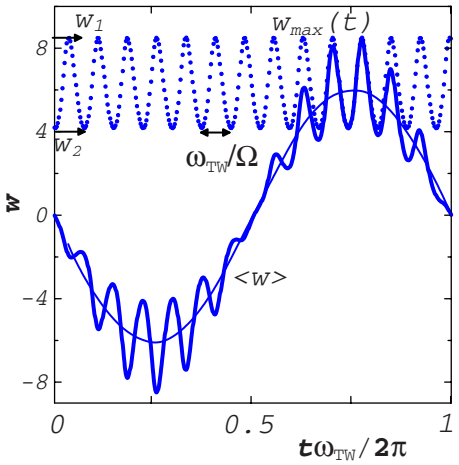

FIG. 2. (Color online) Time evolution of vertical velocity of the amplitude modulated TW identified by arrow A in Fig. 1. Thick line shows $w(t)$ at a fixed location, $(x_0, z_0 = 1/2)$, thin line shows running average $\langle w \rangle(t)$ (2.9), and dotted line the maximum in the whole layer, $w_{\max}(t)$ (2.8). The oscillation range of the latter is indicated by w_1 and w_2. The plot covers one oscillation period $2\pi/\omega_{\mathrm{TW}}$ defined by the largest contribution to the Fourier spectrum of $w(t)$ shown in Fig. 3. Arrows labeled $\omega_{\mathrm{TW}}/\Omega$ indicate the period of the heating modulation. Parameters are $L = 0.01$, $\sigma = 10$, $\psi = -0.25$, $r = 1.281$.

Amplitude modulated TWs are quasiperiodic oscillatory convective states with two different characteristic frequencies, the external driving Ω and a frequency ω_{TW} that characterizes for small modulation amplitude as for $\delta = 0.2$ the main peak in the Fourier spectrum (cf. further below). In general the ratio

$$Q = \Omega/\omega_{\mathrm{TW}} \tag{4.3}$$

is not a rational number. For the TW marked by the arrow A in Fig. 1 at $r = 1.281$ one has $Q = 13.47$.

1. Flow behavior

For this TW we show in Fig. 2 the vertical velocity $w(t)$ at a fixed lateral position, x_0, and at midheight, $z_0 = 1/2$, by a thick line together with its running average $\langle w \rangle(t)$, (2.9). The oscillation of $w_{\max}(t)$, (2.8), indicated by the dotted line in Fig. 2 covers the range from w_2 to w_1. The latter values are shown also in the bifurcation diagram of Fig. 1(a). The maximal vertical flow velocity in a TW is a constant under stationary heating but it oscillates with the period of the modulation of the heating. On the other hand, the running average $\langle w \rangle(t)$, (2.9), of w at a fixed location, (x_0, z_0), oscillates with the frequency ω_{TW} that is shown by the thick line in Fig. 1(b). Note that the mean of $w_{\max}(t)$, (2.8), which is marked by the dot in Fig. 1(a) for $r = 1.281$, is practically given by $w_{\max}$ for stationary driving: The thin line in Fig. 1(a) lies practically in the middle between the thick lines for w_1 and w_2.

The Fourier spectrum of the vertical velocity $w(x_0, z = 1/2, t)$ shown in Fig. 3(a) contains three main contributions. The largest one at ω_{TW}, shown by the thick line in Fig. 1(b), differs at location A only slightly from the unmodulated

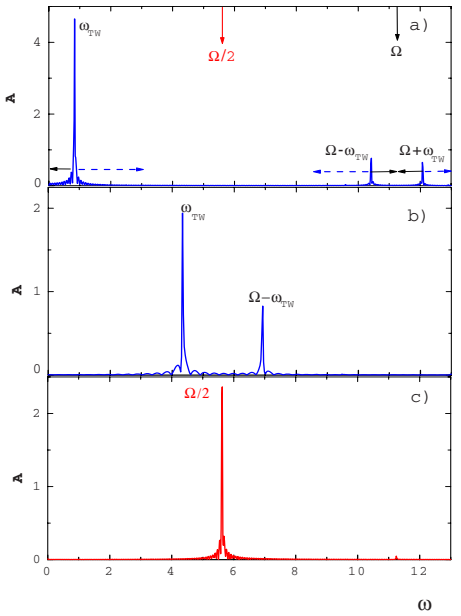

FIG. 3. (Color online) Fourier amplitudes A (in arbitrary units) in the spectrum of $w(x_0,z_0=1/2,t)$ versus frequency ω. (a) Amplitude modulated TW at $r=1.281$ (arrow A in Fig. 1), (b) amplitude and phase modulated TW at $r=1.091$ (arrow C in Fig. 1), and (c) SW at $r=1.087$ (arrow D in Fig. 1). Full (dashed) horizontal arrows indicate how the peaks move when r increases (decreases) as a consequence of the variation of $\omega_{\mathrm{TW}}(r)$ shown in Fig. 1(b).

TW frequency [thin line in Fig. 1(b)]. But when approaching the saddle location r_S^{TW} the difference increases.

The height of the other peaks in the spectrum of Fig. 3(a) are smaller. They are located at the frequencies $\Omega \pm \omega_{\mathrm{TW}}$. They move with increasing (decreasing) r as indicated by the full (dashed) arrows in Fig. 3(a) with ω_{TW} varying as shown in Fig. 1(b). Higher Fourier harmonics in the evolution of $w(x_0,z=1/2,t)$ are very small since the momentum balance equation is only weakly nonlinear. On the other hand, the frequency spectrum of the concentration wave contains significant anharmonicities as one can also infer from the spatial profiles of the C waves discussed in Sec. IV B 2.

For all modulated TWs of Fig. 1 ω_{TW} and the mean phase velocity $\langle v_{ph}\rangle$, (2.11), are related to each other by $\omega_{\mathrm{TW}}=\langle v_{ph}\rangle k$. Furthermore, for amplitude modulated TWs one has $v_{ph}\approx\langle v_{ph}\rangle$. For example, at location A the maximal difference of the phase velocity v_{ph} from its mean value $\langle v_{ph}\rangle$ is 6%.

2. Concentration field

The evolution of the concentration field for the amplitude modulated TW at $r=1.281$ (arrow A in Fig. 1) is shown in Fig. 4 by four shapshots of C in the x-z plane. The times $(a,b,c,d,e)=(0.150,0.185,0.220,0.260,0.775)2\pi/\omega_{\mathrm{TW}}$ correspond to local extrema in the plot of $w(t)$ in Fig. 2. One can see that our TW propagates to the left.

With the phase velocity $v_{ph}=0.265$ being very small compared to the extrema $w_2=4.17$ and $w_1=8.5$ of $w_{\max}(t)$ this TW is a slow [32], strongly nonlinear state with strong advectice mixing of the concentration field [5]: The difference

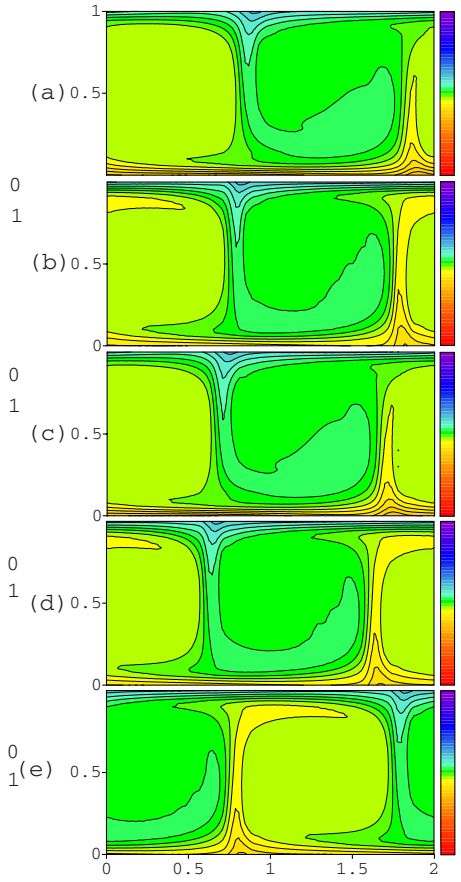

FIG. 4. (Color online) Snapshots of the concentration distribution in the amplitude modulated TW at $r=1.281$ (arrow A in Fig. 1). The times in (a,b,c,d,e) correspond to local extrema of $w(t)$ in Fig. 2 at $(0.150,0.185,0.220,0.260,0.775)2\pi/\omega_{\mathrm{TW}}$, respectively. The vertical color bars show the coding in the unmodulated conductive state with $C^0_{\mathrm{cond}}(z)$ varying linearly from −0.125 at the bottom to 0.125 at the top for $\psi=-0.25$.

between maximal and minimal C is much smaller than in the unmodulated conductive state (color bar on the right-hand side of Fig. 4).

In our left-propagating TW the regions of closed streamlines in the comoving frame for the right (left) turning fluid domains are poor (rich) in ethanol and they are displaced towards the upper cold (lower warm) plate, where the Soret effect maintains a boundary layer with alcohol surplus (deficiency). Furthermore, there are narrow boundary layers between the rolls and close to the plates with large concentration gradients. The fluid becomes diffusively homogenized in the closed-streamline regions of the rolls leading to anharmonic concentration profiles of trapezoidal shape. The motion of the rolls with their specific concentration distribution implies a mean concentration current which is directed to the left in the upper and to the right in the lower one-half of the layer.

C. Harmonic response with fixed phase

When the mean heating rate is increased the TW frequency ω_{TW} decreases as in the absence of modulation.

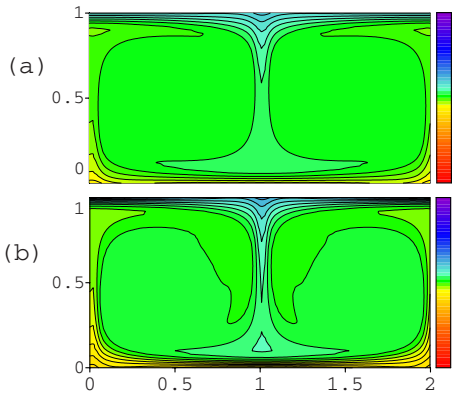

FIG. 5. (Color online) Snapshots of the concentration distribution for phase fixed modulated convection at $r=1.368$ (arrow B in Fig. 1). The vertical flow velocity between the rolls at $x=1$ is maximal in (a) and minimal in (b). The color coding is the same as in Fig. 4.

Thus, the two peaks in the spectra of Fig. 3 at $\Omega \pm \omega_{\mathrm{TW}}$ approach each other as indicated schematically by the full horizontal arrows in Fig. 3(a). At $r=1.368$ the TW frequency ω_{TW} drops to zero, cf. Fig. 1(b). Beyond this r value, a different type of solution appears with phase fixed modulated convection (MC) that oscillates synchronously with the modulated heating: In the regime marked as MC in Fig. 1 only one main peak remains in the Fourier spectrum of $w(x_0, z_0=1/2, t)$ that is located at the externally imposed modulation frequency Ω plus higher harmonics thereof.

In this MC regime, the flow amplitudes basically just oscillate around the unmodulated SOC state's flow. Also the mean of $w_{\max}(t)$, (2.8), is practically given by $w_{\max}$ in the SOC state for stationary driving: The thin line in Fig. 1(a) lies in the middle between the thick lines for w_1 and w_2.

Figure 5 shows two snapshots of the concentration distribution in the layer when the vertical flow velocity at a fixed location, say, between two rolls at $x_0=1$ in Fig. 5 is maximal (a) and minimal (b), respectively. This concentration field looks like the one in SOC states under stationary driving [20] with the mirror symmetry between oppositly turning rolls and with the advective mixing being much stronger than for TWs.

Also here, for modulated heating, $\delta \neq 0$, one observes the $\delta=0$ scenario for the transition from TWs to SOCs: ω_{TW} and v_{ph} decrease since whith increasing r advection increases. Thereby, the regions of closed streamlines grow at the expense of the open ones. Consequently, the former also come closer to the respective opposing horizontal boundary layers. This decreases the asymmetry of the boundary layer feeding into oppositely turning rolls. As a consequence, the concentration contrast between adjacent TW rolls—which drives the lateral phase propagation of the TWs—decreases until in the MC state with $v_{ph}=0$ the rolls are fed symmetrically by both boundary layers and mirror symmetry between the rolls is established.

D. Amplitude and phase modulated traveling waves

Here we return to the quasiperiodic, modulated TWs. We want to discuss in particular the behavior at low r where not only the TW amplitudes but also the phase velocities are modulated significantly and where the concentration dynamics gets quite complex.

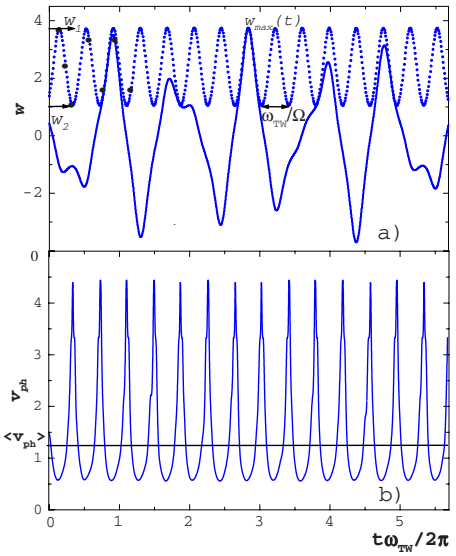

FIG. 6. (Color online) Time evolution of vertical velocity (a) and of the phase velocity (b) of the phase and amplitude modulated TW identified by arrow C in Fig. 1. Full line in (a) shows $w(t)$ at a fixed location, $(x_0, z_0=1/2)$, and dotted line the maximum $w_{\max}(t)$ (2.8) in the whole layer. The oscillation range of the latter is indicated by w_1 and w_2. The plot covers several oscillation periods of ω_{TW} defined by the largest contribution to the Fourier spectrum of $w(t)$ shown in Fig. 3(b). Arrows labeled $\omega_{\mathrm{TW}}/\Omega$ indicate the period τ of the heating modulation. Full horizontal line in (b) is the mean phase velocity $\langle v_{ph} \rangle$ (2.11). Parameters are $L=0.01$, $\sigma=10$, $\psi=-0.25$, $r=1.091$.

The main TW frequency ω_{TW} as identified by the main contribution to the frequency spectrum of $w(x_0, z_0=1/2, t)$ in Fig. 3 increases with decreasing r: With decreasing heating the flow intensity and the advective mixing decreases, the Soret induced diffusive concentration gradients become less washed out, the resulting driving (restoring) forces for oscillations increase, and thus ω_{TW} grows. Consequently, the peaks in Fig. 3 at ω_{TW} and $\Omega-\omega_{\mathrm{TW}}$ approach each other. In Fig. 3(b) we show the spectrum for the TW at $r=1.091$ (arrow C in Fig. 1) at the lower end of the existence interval of modulated TWs. Its frequency $\omega_{\mathrm{TW}}=4.33$ and with it its mean phase velocity $\langle v_{ph}(t) \rangle = \omega_{\mathrm{TW}}/k$ is significantly larger than that of TW A in Fig. 1.

In Fig. 6 we show the time variation of w at a fixed location, of $w_{\max}(t)$, and of the phase velocity $v_{ph}(t)$ of the TW at the arrow C in Fig. 1. The latter two velocities oscillate with the period $\tau=2\pi/\Omega$ of the heating. With the large amplitude oscillations of the phase velocity and with the complicated variation of w in Fig. 6(a)—reflecting the fact that the two frequencies ω_{TW} and $\Omega-\omega_{\mathrm{TW}}$ are close to each other—the flow dynamics of TW C is significantly more complex than that of TW A.

The increase in spatiotemporal complexity is even more dramatic for the concentration field of TW C in comparison to that of TW A, cf. Fig. 7: Since $v_{ph}(t)$ is sometimes larger and sometimes smaller than $w(t)$ or $w_{\max}(t)$ open and closed

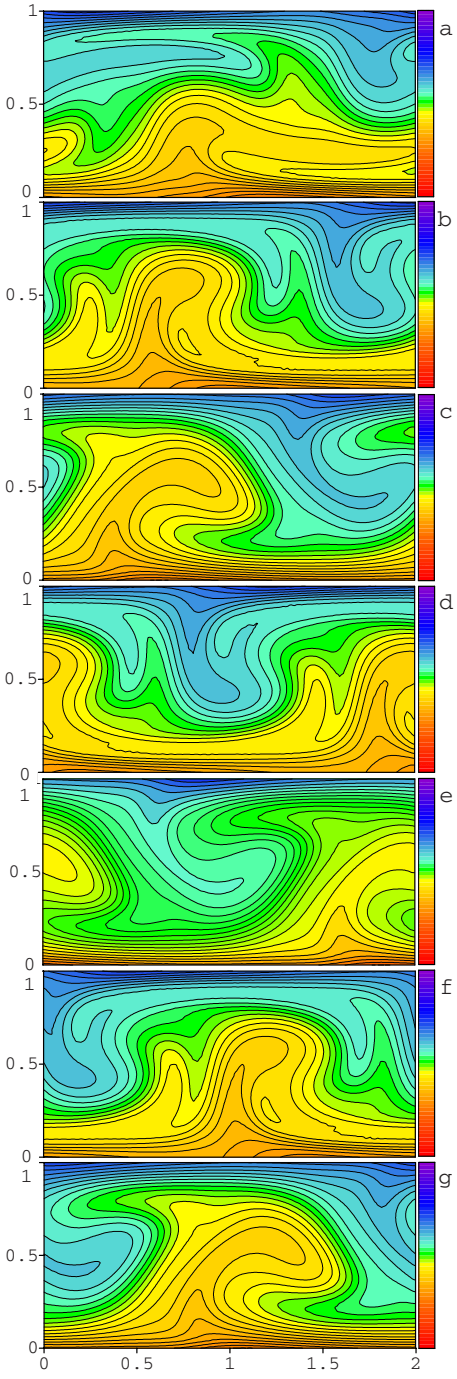

FIG. 7. (Color online) Snapshots of the concentration distribution in the phase and amplitude modulated TW at $r=1.091$ (arrow C in Fig. 1). The times from top to bottom, $(0.138, 0.234, 0.331, 0.569, 0.769, 0.954, 1.154)2\pi/\omega_{\mathrm{TW}}$ can be identified in Fig. 6. The color coding is the same as in Fig. 4.

streamline regions appear alternatingly with the associated advective characteristics [22,35]. The snapshots of C in Figs. 7(a)–7(g) are taken at times $(0.138, 0.234, 0.331, 0.569, 0.769, 0.954, 1.154)2\pi/\omega_{\mathrm{TW}}$ [cf. points in the plot of $w_{\max}(t)$ in Fig. 6(a)]. Figure 7(a) corresponds to the maximum of advective flow velocity and the phase velocity of TW C is minimal in this time. The concentration streamline is opened. In Fig. 7(b) concentration field evolves in TW solution with the roll-like regions of closed streamlines. In the following time interval the advective velocity leads to a minimum and therefore the advective mixing decreases [Fig. 7(c)]. In this case the TW has a maximum of phase velocity. Later on closed [Figs. 7(d) and 7(f)] and open [Figs. 7(e) and 7(g)] streamlines of concentration field alternate.

Note finally that TW C is located well below the saddle location of unmodulated TWs at $r_S^{\mathrm{TW}}(\delta=0)=1.175$. However, with the modulation (4.1) of the thermal driving, $r(t)$ periodically grows beyond $r_S^{\mathrm{TW}}(\delta=0)$ when $\delta=0.2$ as in our case. Thus, $r_S^{\mathrm{TW}}(\delta=0)/1.2$ could be expected to be a lower limit for the existence of modulated TWs.

E. Subharmonic standing waves

We found stable SW convection that oscillates subharmonically with frequency $\omega_{\mathrm{SW}}=\Omega/2$ at small r as indicated by the thick lines labeled SW in Fig. 1. The existence range, $1.0526<r<1.1055$, of these modulation-stabilized SWs lies below the existence range of the unstable unmodulated SWs that are indicated by thin dashed lines in Fig. 1. Note also that there is a small hysteresis in the transitions between TW and SW solutions when one varies the mean heating rate r quasistatically: Modulated TW and SW solutions coexist bistably in the interval $1.091<r<1.105$ (delimited by vertical dotted lines in Fig. 1).

In contrast to the quasiperiodic TWs discussed in Secs. IV B and IV D the SWs are periodic states, i.e., their Fourier spectrum [cf. Fig. 3(c)] contains only the dominant frequency ω_{SW} and its higher harmonics, in particular 2 ω_{SW} and 3 ω_{SW}. The third harmonic being larger in amplitude than the second one lies outside the plot range of Fig. 3(c). The SWs have the mirror-time-shift (MTS) symmetry

$$f(x,z;t) = -f(x,1-z;t+\tau_{\mathrm{SW}}/2) \tag{4.4}$$

with f denoting Ψ, φ, T, or C that is also observed in SWs under stationary heating [20]. Here, in our subharmonic SWs $\tau_{\mathrm{SW}}=2\tau=4\pi/\Omega$. The MTS symmetry reflects the fact that in the SW the left and right turning rolls—which are always mirror images of each other—change periodically their vorticity: After a time $\tau_{\mathrm{SW}}/2$ a left (right) turning roll becomes a right (left) turning one.

Because of MTS (4.4), the Nusselt number $\mathrm{Nu}(t)$ (2.7) and the mixing number $M(t)$ (2.13), both into which enter lateral integrations, have oscillation periods of $\tau_{\mathrm{SW}}/2=\tau$, i.e., their oscillation frequency is the driving frequency Ω.

The SWs are less nonlinear and in particular with respect to their concentration field structure also closer to the quiescent conductive state than the highly nonlinear TWs. In the snapshots of the SW concentration distribution in Fig. 8 the boundary layers are less sharp than, say, in the TW shown in Fig. 4 and the Soret induced concentration contrasts in the SW are much less washed out by nonlinear advection than in the TW: Figure 8 is much more colorful (with a color distribution that is closer to the one in the coding bar for the quiescent conductive state) than the Fig. 4 for TW A which is dominated by the green color representing a better mixed situation with mean concentration. This explains that the mean mixing number $\langle M\rangle$ (2.13) which measures variations

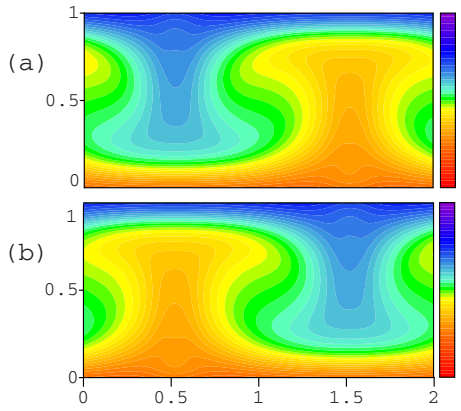

FIG. 8. (Color online) Snapshots of the concentration distribution in the subharmonically oscillating SW at $r=1.087$ (arrow D in Fig. 1). The time difference between (a) and (b) is $\tau_{SW}/2=\tau$. The color coding is the same as in Fig. 4.

of the concentration field is much larger for the SW D ($\langle M\rangle=0.432$) than for the TW A ($\langle M\rangle=0.118$) and also larger, albeit less so, than for the TW C ($\langle M\rangle=0.321$).

F. Fourier dynamics of the flow

To elucidate the spatiotemporal behavior of the different convection types discussed here so far and the transitions between them we used also the diagnostic tool of the lateral Fourier decomposition (2.12) of all fields in particular at midheight position, $z=1/2$. The behavior of the fields there is representative also for other vertical positions. Here we present results for the vertical velocity field. In contrast to the concentration field the lateral variation of w is largely harmonic so that the first Fourier mode $\hat{w}_1$ in the presentation (2.12) of $w(x,z=1/2,t)$ determines the flow behavior.

In Fig. 9 the time evolution of the complex mode $\hat{w}_1(t)$ is shown in the plane spanned by its real and imaginary part, respectively, for various convection types. In the case of the amplitude modulated TW A discussed in Sec. IV B the trajectory of $\hat{w}_1(t)$ in Fig. 9(a) looks like a daisy. The daisy is the projection of the spatiotemporal flow dynamics of the whole TW in real space into Fourier space. It complements the picture of the TW dynamics of w at a fixed location shown in Fig. 2.

The motion of $\hat{w}_1(t)$ in Fig. 9(a) is limited by two circles. Their radii are given by the extrema of $w_{\max}(t)$ [cf. Figs. 1(a) and 2]—i.e., w_1 for the outer radius and w_2 for the inner one, respectively—since w is very well represented by the first lateral Fourier mode $\hat{w}_1$. Without modulation, $w_1=w_2$, the daisy in Fig. 9(a) degenerates to a circle along which $\hat{w}_1(t)$ moves clockwise in the case of a TW propagating to the left. For a TW propagating to the right $\hat{w}_1(t)$ moves counterclockwise.

Since the two characteristic frequencies ω_{TW} and Ω of the modulated quasiperiodic TW A are not rationally related to each other the trajectory of $\hat{w}_1(t)$ is not closed in Fig. 9(a). There we show the time interval of 14 modulation periods which is slightly larger than $2\pi/\omega_{TW}$ since $Q=\Omega/\omega_{TW}=13.47$. In this time $\hat{w}_1(t)$ moves 14 times from the inner to the outer radius and back as a result of the amplitude modulation. The time between successive maxima of $|\hat{w}_1(t)|$ is the period of the temperature modulation. Here the motion of $\hat{w}_1(t)=|\hat{w}_1(t)|e^{i\varphi_1(t)}$ is such that the phase velocity $\dot{\varphi}_1$ is practically constant with $|\dot{\varphi}_1|\approx v_{ph}$.

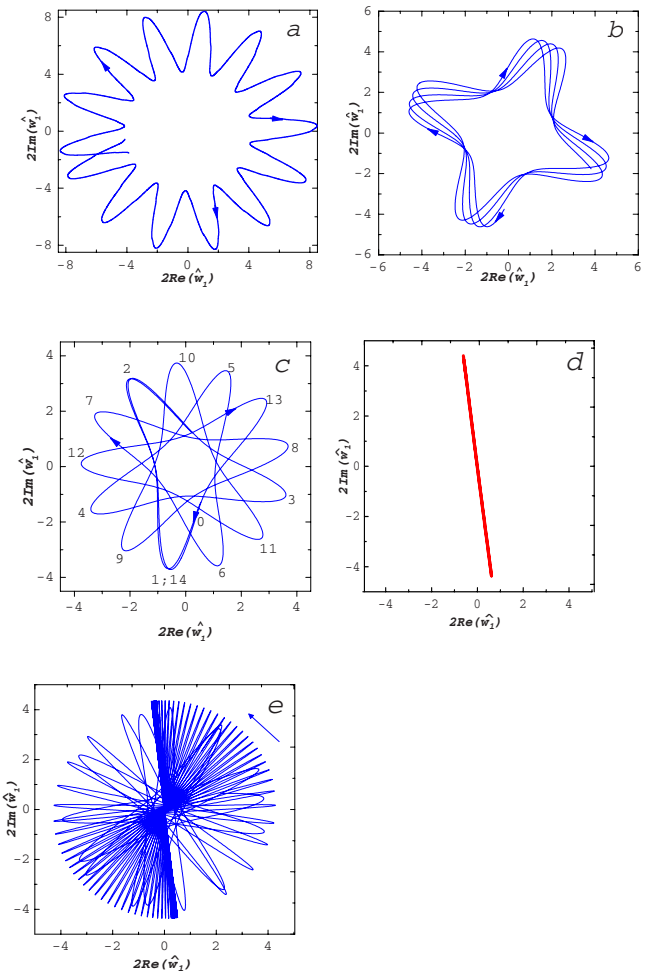

FIG. 9. (Color online) Trajectories of the first lateral Fourier mode $\hat{w}_1(t)$ of the vertical velocity $w(x,z=1/2,t)$ in the plane spanned by the real and imaginary part of $\hat{w}_1$. (a) Amplitude modulated TW A ($r=1.281$, $Q=13.47$), (b) amplitude and phase modulated TW ($r=1.117$, $Q=3.91$), (c) amplitude and phase modulated TW C ($r=1.091$, $Q=2.60$), (d) SW D ($r=1.087$, $\Omega/\omega_{SW}=2$), (e) transient from TW C after decreasing r towards SW D.

With decreasing r the TW frequency ω_{TW} increases [cf. Fig. 1(b)] and Q decreases. In Fig. 9(b) we show the Fourier dynamics of a modulated TW with $Q=3.91$ at $r=1.117$, i.e., somewhat closer to the location of TW C than to TW A covering a time interval of about 15 periods of the driving. Unlike TW A this TW shows a significant modulation of the phase velocity of about 40% around a mean $\langle v_{ph}\rangle=0.912$. Here $|\dot{\varphi}_1|$ is large when $|\hat{w}_1|$ is small.

Figure 9(c) shows TW C with $Q=2.60$ over the same time interval as that of Fig. 6, i.e., also about 15 periods of the modulation. For the convenience of the reader we have indicated the start by 0. Consecutive maxima of $|\hat{w}_1|$ are numbered from 1 to 14. Here we have large oscillations of the amplitude $|\hat{w}_1|$ as well as of the phase velocity $\dot{\varphi}_1$. Again the

latter is very large when $|\hat{w}_1|$ is small—the spikes of $v_{ph}(t)$ in Fig. 6 are located at the minima of $w_{\max}(t)$.

Figure 9(d) shows the motion of $\hat{w}_1(t)$ along a straight line through the origin for the SW D discussed in Sec. IV E. The orientation of the line is given by a constant contribution to the phase that itself is determined, say, by the lateral locations of the extrema of upflow and downflow. This phase location depends on initial conditions and the driving history. In our case the procedure was the following: We took as initial condition the modulated TW C at $r=1.091$ and then reduced r instantaneously to $r=1.090$ lying slightly below the existence range of modulated TWs.

The transient from the modulated TW to the SW D subsequent to this driving step is shown in Fig. 9(e). At first one can see the trihedral shape of the trajectory as traced out along the points 1,2,3 in the TW C in Fig. 9(c). Then these trihedrons elongate as the maxima of $|\hat{w}_1|$ grow towards the SW value being larger than that of TW C [cf. Fig. 9(a)]. After that the shape of the trajectory rapidly transforms into a thin ellipsoidal form which itself rotates counterclockwise as indicated by the arrow in Fig. 9(e). The ellipses become thinner and thinner and the phase difference between successive maxima of $|\hat{w}_1|$ decreases until the trajectory locks into the straight line of the stable SW in Fig. 9(d).

V. CONCLUSION

The spatiotemporal behavior and the bifurcation properties of oscillating convection rolls in binary fluid mixtures subject to sinusoidal modulation of the lower boundary's temperature have been investigated with finite difference numerical simulations. The simulations have been performed for parameters adapted to experiments that use ethanol-water mixtures with sufficiently negative Soret coupling to show subcritical Hopf bifurcations into TWs and SWs. Various diagnostic and visualization tools have been used to elucidate the spatiotemporal structure and bifurcation properties of the rich and rather complex, strongly nonlinear response behavior to modulation of the thermal driving. The richness and complexity is partly due to the fact that subcritically bifurcating convection of sizeable amplitudes is already without modulation strongly nonlinear because of the advection dominated concentration dynamics. With temperature modulation the bouyancy induced advection gets modulated and leads in particular for the modulated TWs to complex nonlinear mixing behavior. However, all solutions investigated here displayed the mirror-glide symmetry (4.2).

When modulating with a frequency Ω that is large compared to the TW frequencies under stationary driving, $\delta=0$, we found the following different response characteristics depending on r: (i) Stable SOC states occuring for $\delta=0$ at large $r>r^*$ become synchronously modulated and oscillate with fixed phase around the SOC solution. (ii) The TWs shortly below the upper existence limit r^* of unmodulated TWs experience basically only a modulation of their amplitude thus becoming quasiperiodic states. (iii) With decreasing r the TW phase velocity v_{ph} becomes modulated more and more as well. Here, the mixing behavior of the concentration is very complex with open and closed streamline regions appearing alternatingly. The existence range of these modulated TWs extends down to r values well below the saddle location r_S^{TW} of unmodulated TWs. Thus, modulation stabilizes TW convection. (iv) At the lower end of the r range of modulated TWs there is a hysteretic transition to subharmonic SWs. These periodic states are frequency locked over a finite r interval to oscillate with half the modulation frequency and they show the mirror-time-shift symmetry (4.4). The modulation stabilized SWs occur below the saddle r_S^{SW} of unstable unmodulated SWs. They are less nonlinear and—in particular with respect to their concentration field structure—closer to the quiescent conductive state than the highly nonlinear TWs.

ACKNOWLEDGMENTS

This work was supported by the Russian Basic Research Foundation (Contract No. 07-01-96040) and by the DAAD (Forschungsaufenthalte für Hochschullehrer und Wissenschaftler, 2008–2009).

[1] M. C. Cross and P. C. Hohenberg, Rev. Mod. Phys. **65**, 851 (1993).
[2] For 5 weight percent of ethanol mixed into water at $T=20\,^{\circ}\mathrm{C}$ the separation ratio measuring the Soret coupling strength [1] is $\psi\simeq-0.3$ [3].
[3] P. Kolodner, H. L. Williams, and C. Moe, J. Chem. Phys. **88**, 6512 (1988).
[4] R. W. Walden, P. Kolodner, A. Passner, and C. M. Surko, Phys. Rev. Lett. **55**, 496 (1985).
[5] M. Lücke, W. Barten, P. Büchel, C. Fütterer, St. Hollinger, and Ch. Jung, in *Evolution of Structures in Dissipative Continuous Systems*, edited by F. H. Busse and S. C. Müller, Lecture Notes in Physics, Vol. 55 (Springer, Berlin, 1998), p. 127.
[6] E. Moses, J. Fineberg, and V. Steinberg, Phys. Rev. A **35**, 2757 (1987); R. Heinrichs, G. Ahlers, and D. S. Cannell, *ibid.* **35**, 2761 (1987).
[7] K. E. Anderson and R. P. Behringer, Phys. Lett. A **145**, 323 (1990); K. E. Anderson and R. P. Behringer, Physica D **51**, 444 (1991).
[8] B. I. Winkler and P. Kolodner, J. Fluid Mech. **240**, 31 (1992).
[9] P. Kolodner, Phys. Rev. E **50**, 2731 (1994).
[10] H. Touiri, J. K. Platten, and G. Chavepeyer, Eur. J. Mech. B/Fluids **15**, 241 (1996).
[11] E. Kaplan, E. Kuznetsov, and V. Steinberg, Phys. Rev. E **50**, 3712 (1994).
[12] C. M. Surko, D. R. Ohlsen, S. Y. Yamamoto, and P. Kolodner, Phys. Rev. A **43**, 7101 (1991).
[13] C. M. Aegerter and C. M. Surko, Phys. Rev. E **63**, 046301 (2001).
[14] L. Ning, Y. Harada, and H. Yahata, Prog. Theor. Phys. **98**, 551

(1997).
[15] O. Batiste, E. Knobloch, I. Mercader, and M. Net, Phys. Rev. E **65**, 016303 (2001).
[16] D. Jung and M. Lücke, Phys. Rev. Lett. **89**, 054502 (2002); Phys. Rev. E **72**, 026307 (2005).
[17] D. Bensimon, P. Kolodner, C. M. Surko, H. Williams, and V. Croquette, J. Fluid Mech. **217**, 441 (1990).
[18] P. Kolodner, Phys. Rev. A **46**, 6452 (1992).
[19] P. Matura, D. Jung, and M. Lücke, Phys. Rev. Lett. **92**, 254501 (2004).
[20] D. Jung, P. Matura, and M. Lücke, Eur. Phys. J. E **15**, 293 (2004).
[21] W. Barten, M. Lücke, M. Kamps, and R. Schmitz, Phys. Rev. E **51**, 5636 (1995); **51**, 5662 (1995).
[22] C. Fütterer and M. Lücke, Phys. Rev. E **65**, 036315 (2002).
[23] M. I. Shliomis and B. L. Smorodin, Phys. Rev. E **71**, 036312 (2005).
[24] A. Alonso and O. Batiste, Theor. Comput. Fluid Dyn. **18**, 239 (2004).
[25] G. Z. Gershuni and E. M. Zhukhovitsky, *Convective Stability of Incompressible Fluids* (Keter, Jerusalem, 1976).
[26] P. M. Gresho and R. L. Sani, J. Fluid Mech. **40**, 783 (1970).
[27] G. Venezian, J. Fluid Mech. **35**, 243 (1969).
[28] S. Rosenblat and G. A. Tanaka, Phys. Fluids **14**, 1319 (1971).
[29] C. S. Yin and C. H. Li, J. Fluid Mech. **54**, 143 (1972).
[30] G. Ahlers, P. C. Hohenberg, and M. Lücke, Phys. Rev. A **32**, 3519 (1985).
[31] G. Ahlers, P. C. Hohenberg, and M. Lücke, Phys. Rev. A **32**, 3493 (1985).
[32] St. Hollinger and M. Lücke, Phys. Rev. E **57**, 4238 (1998).
[33] L. D. Landau and E. M. Lifschitz, *Course of Theoretical Physics* (Pergamon, Oxford, 1993), Vol. 6.
[34] J. K. Platten and J. C. Legros, *Convection in Liquids* (Springer, Berlin, 1984).
[35] St. Hollinger, P. Büchel, and M. Lücke, Phys. Rev. Lett. **78**, 235 (1997).